

Comprehensive Bayesian structural identification using temperature variation

Andre Jesus^{a,*}, Peter Brommer^{b,c}, Yanjie Zhu^a, Irwanda Laory^{a,*}

^a*Civil Research Group, School of Engineering, University of Warwick, Coventry CV4 7AL UK*

^b*Warwick Centre for Predictive Modelling, School of Engineering, University of Warwick, Coventry CV4 7AL, UK*

^c*Centre for Scientific Computing, University of Warwick, Coventry CV4 7AL, UK*

Abstract

A modular Bayesian method is applied for structural identification of a reduced-scale aluminium bridge model subject to thermal loading. The deformation and temperature variations of the structure were measured using strain gauges and thermocouples. Feasibility of a practical, temperature-based, Bayesian structural identification is highlighted. This methodology used multiple responses to identify existent discrepancies of a model, calibrate the stiffness of the bridge support and establish uncertainty of a predicted response. Results show that the inference of a structural parameter is successful even in the presence of substantial modelling discrepancies, converging to its true physical value. However measurements should have a high dependency on the calibration parameters. Usage of temperature variations to perform structural identification is highlighted.

Keywords: Bayesian inference, model calibration, structural-identification, identifiability, temperature variation

1. Introduction

The capability of a structural health monitoring (SHM) system to interpret monitored data is the main factor that dictates its performance and its usefulness to owners and local authorities.

Interpretation of the data using a physics-based model is advantageous because its development and usage as a predictive tool agrees with engineering knowledge, making it more understandable. However the main disadvantage is that the model has to be calibrated, before it can be used as a predictive tool. Moreover, using a deterministic model, i.e. a model where input parameters and

*Corresponding author

Email addresses: andrehejesus@openmailbox.org (Andre Jesus),
I.Laory@warwick.ac.uk (Irwanda Laory)

response outputs are deterministic, rarely correlates well with real data, due to the complexity and inherent uncertainties of this latter one. Hence in most situations a probabilistic approach is more realistic [1] and methods such as model falsification [2], fuzzy numbers [3], Kalman filters [4], sampling methods [5], Markov processes [6] amongst others [7] have been developed for this purpose.

Bayesian inference is the basis of a class of well known methods which also allow to perform structural identification. Beck [8, 9] is known as one of the pioneers of the application of Bayesian methods in SHM. Numerous research works have been conducted on the basis of this initial framework [10, 11]. Based on this research, two fundamental problems might be thought as to why Bayesian methods were not widely applied in SHM practice. Firstly, the model parameters to be calibrated are often assumed as fixed physical properties of the infrastructure, while in reality these properties change due to external factors such as traffic and environmental variations [12], e.g. stiffness of the structure. Secondly, uncertainties due to modelling errors are only partially considered, despite being ubiquitous. They can be caused by: (a) discrepancy between the behaviour of a physics-based model and that of the real structure; and (b) numerical error in solving the partial differential equations (e.g. finite element method and mesh discretization). Component (a) is extremely difficult to quantify. Most of the present research [13, 14] usually disregard this form of uncertainty or consider it as zero mean Gaussian distributed [6]. Only a limited number of authors in the SHM community, namely Higdon [15] and Simoen [16] have applied Bayesian methodologies under this scope. Model-based Bayesian structural identification with temperature variations is also considerably scarce in the literature [17, 12].

Higdon applied a comprehensive modular Bayesian method originally developed by Kennedy and O'Hagan (KOH) [18, 19], which was not widely accepted, presumably because of a lack of identifiability [20, 21]. Identifiability is understood as the capability of inferring the true value of model parameters that represent a physical property, e.g. Young modulus, based on available data. Arendt et al. [22] suggested an improvement to the KOH original formulation to solve the identifiability problem, by using monitored data with diversified responses. This approach was validated on a simulated simply supported beam. We believe that this formulation is very comprehensive to quantify existent uncertainties and superior in some aspects to the ones used in previous works.

Based on this resurgent interest of the modular Bayesian method, the present work focus on its practical application for structural identification using thermal variations. Studies on advantages of using temperature loading for structural identification can be found in the works of Laory [23, 24] and Yarnold [25]. The objective at hand is to test the performance of the improved algorithm on a scale aluminium bridge model subject to thermal loading. To the best of our knowledge this test is the first practical application of this methodology, particularly for temperature based structural identification.

Some of the advantages of using a scale model case study are: more realistic conditions, e.g. noise, inherent randomness and residual deformation of temperature loading; known structural parameters can be used to test the reliability of the methodology; possibility of easily testing different measurement

scenarios; damaging the structure is permissible and allows to easily test damage identification methodologies.

This paper is organised as follows: In section 2, a description of the model calibration formulation is given; section 3 describes the aluminium bridge and its finite element (FE) model, presents a sensor placement analysis, application of the method and its results, and finally, section 4 highlights the conclusions of the present work.

2. Model calibration formulation

This section describes the model calibration approach. A more detailed description can be found in [22]. An introduction to Gaussian process emulation is presented in Appendix A. An outline of the general formulation is given in the next subsection followed by a brief overview of the algorithm and of the numerical approach. To a more in depth description of the uncertainties considered by this methodology see Section 2 of [20].

2.1. Observation and numerical model equations

Let us now assume that a given continuous process ξ has n observations of q responses \mathbf{Y}^e and is dependent on d design variables \mathbf{X}^e . Its observation equation can be written as

$$\mathbf{Y}^e(\mathbf{X}^e) = \boldsymbol{\xi}(\mathbf{X}^e) + \boldsymbol{\varepsilon} \quad (1)$$

where $\boldsymbol{\varepsilon}^T = [\varepsilon_1, \dots, \varepsilon_n]$ is an observation error that is assumed to follow a Gaussian distribution $\mathcal{N}(\mathbf{O}, \boldsymbol{\Lambda})$. On the other hand the unobservable process $\boldsymbol{\xi}(\mathbf{X}^e)$ is described using a numerical model \mathbf{Y}^m as follows

$$\boldsymbol{\xi}(\mathbf{X}^e) = \mathbf{Y}^m(\mathbf{X}^e, \boldsymbol{\theta}^*) + \boldsymbol{\delta}(\mathbf{X}^e) \quad (2)$$

where $\boldsymbol{\delta}(\mathbf{X}^e)$ is a discrepancy function that translates the difference between the model and the true process, $\mathbf{Y}^m(\mathbf{X}^e, \boldsymbol{\theta}^*)$ is the model output and $\boldsymbol{\theta}^*$ are a r -dimensional vector of structural parameters. This equation is an ideal state of the model (i.e. the model is successfully calibrated) when the model parameters $\boldsymbol{\theta}$ take the values $\boldsymbol{\theta}^*$. Although our example updates only one parameter, the methodology can also consider multiple parameters, which is a common scenario in civil infrastructures [26, 27, 13].

It is important to mention that the discrepancy function is independent of the model output and is an unknown of the problem as well as the structural parameters. Now substituting equation number 2 in equation number 1 results in

$$\mathbf{Y}^e(\mathbf{X}^e) = \mathbf{Y}^m(\mathbf{X}^e, \boldsymbol{\theta}^*) + \boldsymbol{\delta}(\mathbf{X}^e) + \boldsymbol{\varepsilon} \quad (3)$$

which is the fundamental equation of the model calibration. Equation number 3 represents the process output to an input \mathbf{X}^e within a domain of a calibrated status $\boldsymbol{\theta} = \boldsymbol{\theta}^*$, representing the best fit with the observed data.

The numerical model and the discrepancy function shall now be replaced by multiple response Gaussian processes (mrGp), whose hyperparameters have to be determined (see the Appendix for a definition and details). These hyperparameters characterise the mrGps and account for an approximation of its associated uncertainties, such as: variability of the numerical model; modelling discrepancies and observation error.

One way of determining the hyperparameters is by applying a Bayesian approach, which fully accounts for all the considered uncertainties and determines all the hyperparameters at the same time. However this implies a significant computational effort and is not recommended [28]. Instead a modular Bayesian approach shall be used, and is described in the following section.

2.2. Modular Bayesian approach

A modular Bayesian approach (MBA) separates the calibration process into four modules, on which the mrGp hyperparameters are estimated separately and progressively [29] as detailed in Fig. 1 (based on Fig. 5 from [20]).

Fixing the hyperparameters at an estimated value reduces the degree of approximation of the uncertainties covered by the mrGp. By doing so, the ‘second order’ effect of those uncertainties is being neglected. This means that preference has been given to recognise all of these sources of uncertainty, to a certain extent at a lower computational cost, rather than fully accounting for the uncertainties, with a considerable increase of computational effort.

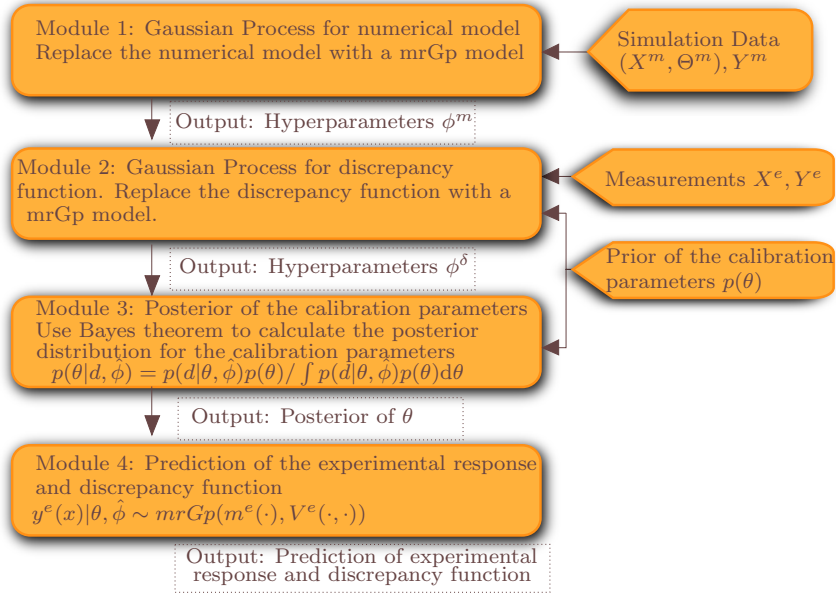


Figure 1: Flowchart of the modular Bayesian algorithm, source [20].

This act of estimating and fixing the hyperparameters is applied progressively, when moving from module 1 to module 2 and from module 2 to module 3. Estimation is done with numerical optimisation methods by maximising the likelihood between the mrGp and the available data.

In our case we used a matlab genetic algorithm (GA) routine. An initial population of size 40 was generated in the $[0-1]$ range, with default values for Gaussian mutation function (mean 0, standard deviation 1 and shrinkage of the standard deviation as generations go by 1) and scattered crossover function (0.8 fraction of the population at the each next generation). Convergence criteria are set as either a maximum number of 100 generations or an average change in the fitness value less than 1×10^{-6} .

It is important to stress that the discrepancy function is not being updated i.e. it is not the same as a GA fitness function. Instead the GA in module 2 (see Fig. 1) aims to estimate the parameters of a statistical model (a Gaussian process), that approximates the discrepancy function. This is done through maximum likelihood estimation (MLE), which implies that the fitness function of the GA is the likelihood function.

In module 3, Bayes' theorem is used for approximating the posterior distribution of θ . In contrast to other approaches mentioned in the introduction, its likelihood function contains the two mrGp approximated in modules 1 and 2, now with its hyperparameters fixed.

3. Aluminium bridge subjected to thermal loading

In this case-study a reduced-scale laboratory aluminium bridge inspired by the New Joban Line Arakawa (Japan) railway bridge, was built at the Warwick Civil Engineering Laboratory and subjected to thermal loading due to infrared heaters. Typical daily ambient temperature in the laboratory ranged from 291.15 K up to 294.15 K. A numerical model of the structure was also developed to study the phenomena. The stiffness of a pair of springs located at one of the ends of the bridge will be considered as a model parameter to be calibrated. Subsection 3.3 details a combinatorial analysis to select the best out of a set of available inputs, to maximise the performance of the method, which is subsequently applied and results are shown in subsection 3.4.

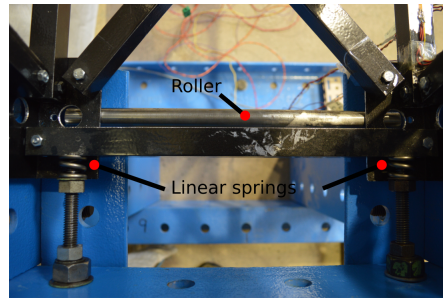
3.1. Experiment

The truss structure in Fig. 2(a) is simply supported at its ends, being constrained on one of them by two linear springs Fig. 2(b) (supplier reference value is $K = 552.26$ N/mm).

Geometrical information and the measurement setup of the bridge are displayed in Fig. 3. Material properties of the bridge are: aluminium alloys of grading 1050AH14 and 6082T6 for the gusset plates and for the box section beams, respectively. Stainless steel M6 8.8 bolts connect the multiple members of the bridge. Eleven strain measurements and four thermocouple readings

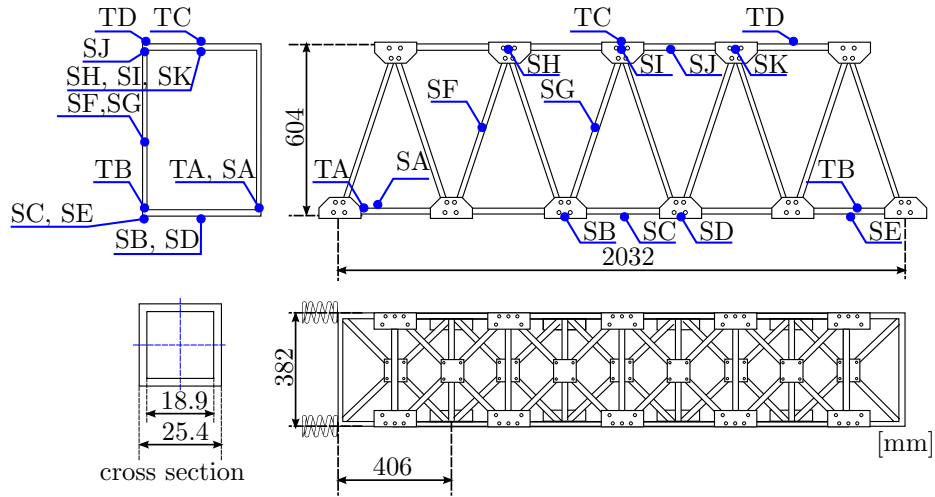


(a)



(b)

Figure 2: Aluminium bridge subjected to thermal loading (a) and detail - springs constraint (top view) (b).



were made during the experiment, at a sampling rate of 1 Hz. A proportional-integral-derivative (PID) controller on a Labview routine was used to control the infrared heaters.

Temperature and strain readings during the main experiment, which took approximately half an hour, are displayed in Figs. 4(a) and 4(b). The reason why the strain even at the top is in compression, is that all the strain gauges have been placed on the bottom side of the bars. Therefore, despite the global bending of the structure that leaves the top bars in traction there is a localised bending at the top bars, which is measured as a compression on their bottom side.

The temperature-strain relation visible on Fig. 4(b) is not linear, because the measurements are performed on the surface of a squared hollow section, which cools down faster than the internal cross section and will, therefore, still have some residual thermal deformation when cooling down.

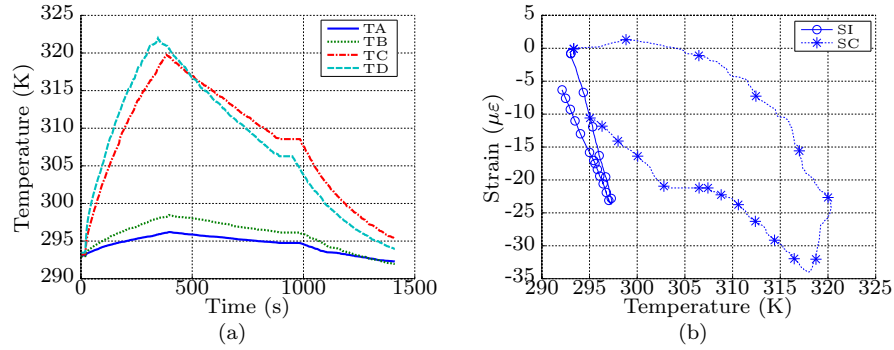


Figure 4: Aluminium bridge heating/cooling cycle - Temperature readings (a) and strain measurements (b), see Fig. 3 for reference.

Although the strain gauges are thermally compensated for aluminium, the data from the strain gauges has been post-processed to remove the remnant thermal output effect, which is related to the natural thermal expansion of the gauge.

3.2. Finite Element model

In this section a FE model of the scale aluminium bridge is presented. The model was developed on ANSYS and coded with APDL (ANSYS parametric design language) [30]. Beam elements with rotational stiffness were used to represent the bars of the bridge. The material model is isotropic, linear-elastic with Young modulus $E = 70 \times 10^6$ kPa, Poisson coefficient $\nu = 0.35$ and coefficient of thermal expansion $\alpha = 23.1 \times 10^{-6} \text{ K}^{-1}$, as standard aluminium. Reference temperature was set as $T_0 = 293.15$ K. A uniform distribution of temperature was applied through all the bar elements, and is based on the mean of the thermocouple measurements at the top of the bridge seen in Figure 4(a).

Essentially nine linearly spaced points of thermal loading from 293.34 K to 318.64 K were simulated as a quasi-static analysis, with different values of the spring stiffness. Each analysis took approximately 0.128 seconds.

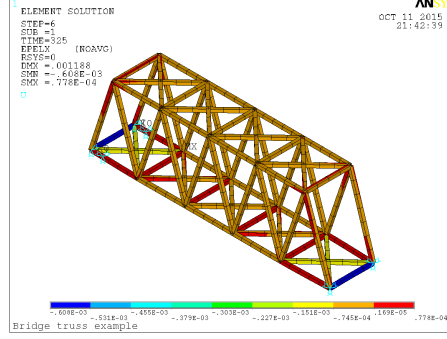


Figure 5: FE model with linear springs at support, maximum temperature of heating cycle.

Figure 5 shows the strain output of the bridge model for this loading condition. It is considerably easier to model the infrastructure behaviour with a uniform temperature gradient on all of its elements, but obviously this is a model discrepancy, since in the laboratory experiment the top of the bridge is much hotter than the bottom side, as seen in Figure 4(a). Since the strain of the FE model is being sampled at the bottom side of the top bars the effect of the localised bending should be relatively small on the results.

3.3. Sensor location combinatorial analysis

This section presents a study of the influence of sensor location on the capability of inferring the spring stiffness true value.

The modular Bayesian approach was applied to infer this parameter, based on all possible combinations of two out of eleven strain measurements available from the laboratory experiment. Only the first three modules of the algorithm are necessary for this combinatorial analysis. The resulting posterior distribution is a Gaussian-shaped distribution whose moments (mean value and standard deviation) estimate the stiffness value. Therefore of the $C_2^{11} = 55$ possible combinations, the ones with minimum standard deviation $\sigma[\theta]$ and expected value $E[\theta]$ closer to the spring stiffness real value were selected. This is possible only because in this example the true value is known, and $\epsilon(\%)$ can be determined.

Input data is given in Table 1 and the output are the moments from the posterior distribution of the spring stiffness. Table 2 displays the results with a relative error $\epsilon = \frac{|K - E[\theta]|}{K} \leq 10\%$. The successful convergence by change in the fitness value (Yes or No in the right column) of the genetic algorithms for the maximum likelihood optimisation of module 2 is also shown. On the other hand Table 3 shows the results obtained for standard deviations $\sigma \leq 70$ N/mm. Finally the worst values of metrics for σ and ϵ were 171.87 N/mm and 43.18 %, respectively.

Parameter	Description
\mathbf{X}^e	13 readings of temperature at the top of the bridge (mean of TC and TD, Fig. 4(a)) from the beginning of the heating cycle until its maximum
\mathbf{Y}^e	strain measurements at points B and G (Fig. 3) for each of the temperature readings
θ	spring stiffness with $\theta^* = 552.26$ N/mm
$[\mathbf{X}^m, \Theta]$	combination set of each temperature reading with possible spring stiffness values on a 9×9 input grid space with $K[300; 1000]$ N/mm and $T[293.3; 319.9]$ K
\mathbf{Y}^m	simulations from the numerical model for $[\mathbf{X}^m, \Theta]$

Table 1: Dataset for aluminium bridge.

S1	S2	E[θ]	$\epsilon(\%)$	$\sigma[\theta]$	GA	S1	S2	E[θ]	$\epsilon(\%)$	$\sigma[\theta]$	GA
A	H	605.04	9.56	171.87	Y	D	H	520.64	5.72	147.19	Y
A	I	596.49	8.01	169.60	Y	H	I	603.12	9.21	169.62	Y
A	J	602.45	9.09	171.56	N	H	J	599.60	8.57	170.28	Y
A	K	603.98	9.37	170.29	Y	H	K	603.99	9.37	161.07	Y
B	G	532.03	3.66	47.72	Y	I	J	598.17	8.31	169.46	Y
C	E	547.31	0.90	102.21	Y	I	K	604.15	9.40	168.44	Y
D	G	533.90	3.33	126.47	Y	J	K	599.37	8.53	169.94	Y

Table 2: Results of inference of the spring stiffness for different measurement combinations and $\epsilon \leq 10\%$.

S1	S2	E[θ]	$\epsilon(\%)$	$\sigma[\theta]$	GA	S1	S2	E[θ]	$\epsilon(\%)$	$\sigma[\theta]$	GA
A	C	430.84	21.99	58.79	N	D	F	433.96	21.42	65.98	Y
A	F	444.54	19.51	68.20	N	F	G	640.50	15.98	67.50	Y
A	G	687.24	24.44	47.97	N	F	I	439.67	20.39	65.44	Y
B	D	394.75	28.52	68.56	Y	G	H	681.50	23.40	52.91	Y
B	G	532.03	3.66	47.72	Y	G	I	684.32	23.91	50.80	Y
C	G	608.89	10.25	58.89	Y	G	J	676.23	22.45	55.87	Y
C	I	437.85	20.72	56.95	Y						

Table 3: Results of inference of the spring stiffness for different measurement combinations and $\sigma \leq 70$ N/mm

respectively. The results show that:

- the combination of responses measured at point B and G provide the lowest error and variance on the inference of the spring stiffness;
- typically combinations involving measurements near bridge ends (A and E) either present a high variance (notice that no combination with E is

present on Table 3), or the genetic algorithm optimisations do not converge (see the N on the GA column of Table 3). This indicates that measurements near model singularities such as supports tend to present poor identifiability;

- in general combining one measurement from the bridge bottom with one of the middle or top gives the lowest error and variances, which indicates that combining locations with a different loading range enhances identifiability.

To further support this interpretation, a comparison between an identifiability metric applied by Arendt [22] in his simulation, against our example shall be carried out in the following section.

3.4. Model calibration results and discussion

Considering the above results, the FE model was calibrated against the laboratory scale aluminium bridge. The design variable, response outputs and structural parameter are similar to what was presented for the combinatorial analysis in Table 1. The polynomial regression functions are set as $\mathbf{H}(\bullet) = 1$ and the prior of θ as a uniform probability density function (PDF). For this example the computational effort took 16.50 s on an Intel i7 quadcore 2.2 GHz, 6 GB of RAM and an SSD drive.

A mrGp of the model is presented in Figs. 6(a) and 6(b), for the response surface of the strain at locations B and G. Hyperparameters are shown in Appendix B. Notice how the uncertainty shrinks and increases relatively to the distance to the input dataset, to account for the uncertainty of the numerical model.

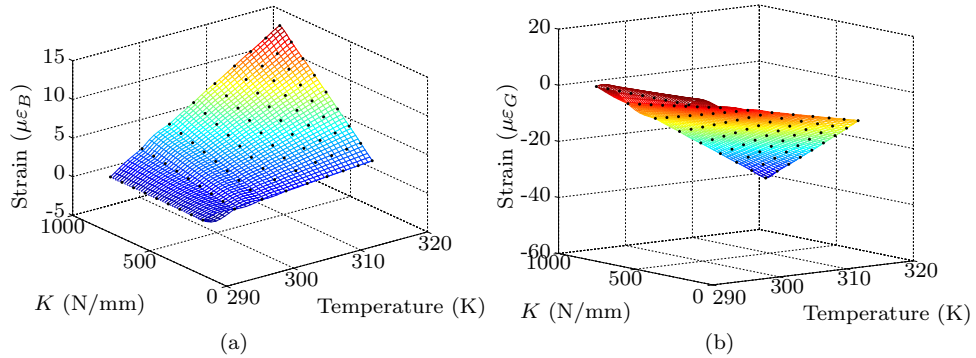


Figure 6: 95 % prediction interval of the posterior multiple response Gaussian process - 40×40 grid with 9×9 grid input set (black dots) of strain at B 6(a) and G 6(b).

The result of the identification task (i.e. inference of the spring stiffness) is shown in Figure 7. A deterministic model identification approach, based on the minimum value of the sum of root mean squared errors of the two signals, leads

to a stiffness value of $K = 661.5$ N/mm with an error of $15.16 \mu\epsilon$. This error is more than five times larger than that of MBA (i.e. $2.82 \mu\epsilon$). Furthermore as seen in Figure 7(b), the stiffness value resulting from MBA, 532.03 N/mm, is closer to the real value of stiffness given by the supplier 552.26 N/mm compared to the stiffness identified using the deterministic model identification. These results demonstrate the superior performance of MBA not only in terms of identifiability but also in the ability to predict structural responses. Despite the fact that the responses used for identification have the same characteristic nature (i.e. strain) the mean value and the variance closely approximate the real stiffness value. It is expected that if other responses such as displacements were given as input this uncertainty would be further improved.

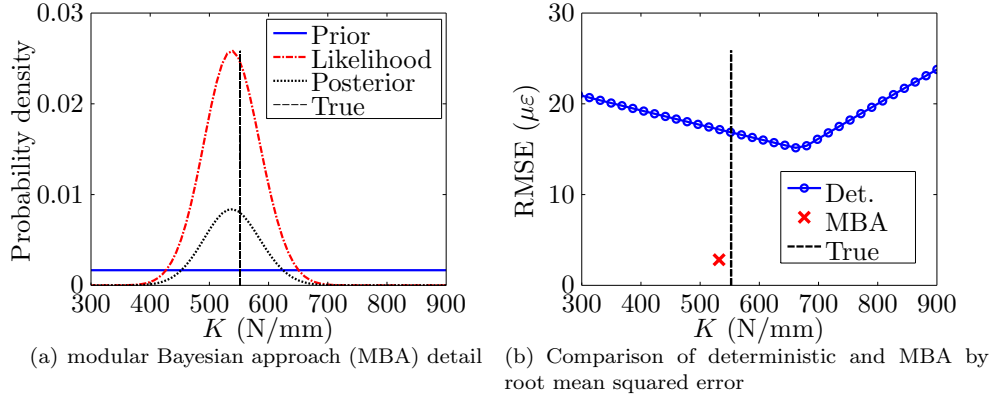


Figure 7: Inference of the stiffness of linear springs at aluminium bridge end, against reference value (vertical dashed line).

In comparison to the hierarchical Bayesian framework from Behmanesh [12] which had an estimation of model parameters with modelling errors at almost 20 % deviation from the true values (see Table 3 for clarification), our estimate deviated only by 3.66 %.

Also to further justify that the improvement on identifiability was achieved, mainly due to the sensor position and not the nature of the measured responses, a comparison between Arendt’s metric in his simulated example and our analysis was applied here. Essentially an improvement of identifiability by using multiple responses should be quantifiable through the posterior standard deviation of the model parameter that is being calibrated, following the formula $(\sigma_{i,j,\min}^{\text{SR}} - \sigma_{i,j,\text{post}}^{\text{MR}}) / \sigma_{i,j,\min}^{\text{SR}}$ where $\sigma_{i,j,\min}^{\text{SR}} = \min(\sigma_{i,\text{post}}, \sigma_{j,\text{post}})$ is the minimum posterior standard deviation of the calibrated parameter with individual responses and $\sigma_{i,j,\text{post}}^{\text{MR}}$ is the posterior standard deviation with multiple responses. In our case an improvement of 10.1 % was observed which is similar to that of 14 % obtained by Arendt (see Table 3 of [22]), on his simply supported beam for responses with similar nature.

Based on the inference of the spring stiffness the mrGp metamodel predic-

tions for strain B and G are shown in Figure 8 and 9, respectively. Notice how the strain at B is positive for the model while negative in the experiment, and how the considerable discrepancy was predicted accurately on Figure 8(b). The solid lines with diamond markers represent the measured response, which is within the uncertainty region. Since this region accounts for: uncertainty of the spring stiffness; model discrepancy; noise and the fact that the model response is known only at a set of discrete points (code uncertainty), the true undisturbed process should also fall within that limit with a 95 % accuracy.

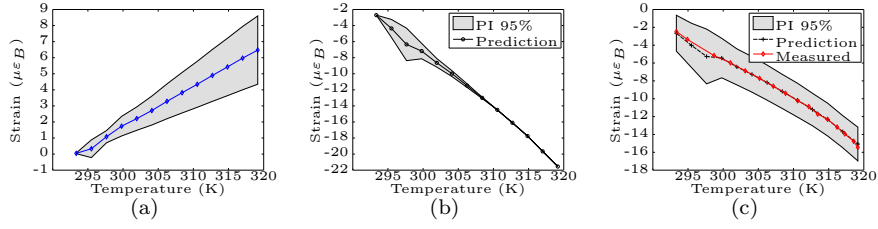


Figure 8: Strain at position B - Prediction interval 95 % confidence for numerical model 8(a), discrepancy function 8(b) and experimental response 8(c).

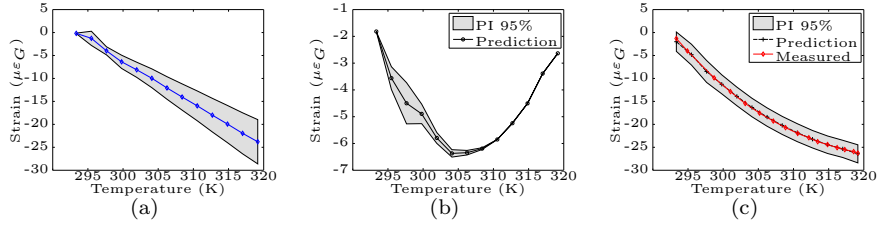


Figure 9: Strain at G aluminium bridge - Prediction interval 95 % confidence for numerical model 9(a), discrepancy function 9(b) and experimental response 9(c).

4. Conclusions

This work applies a modular Bayesian approach on a structural identification framework. A combinatorial analysis to determine the best choice of a set of available sensors which maximises the identifiability of the problem was also performed. Afterwards, with these measurements a simplified model was calibrated against a reduced scale aluminium bridge experiment.

Based on the results the following conclusions can be inferred:

- The methodology is able to identify the true value of a structural parameter and predict responses, while considering uncertainties due to parametric variability, observation error, residual variability, code variability and model discrepancy for an experimental setup;

- It is possible to infer a fixed structural parameter with only two measurements of a single characteristic nature, even in the presence of high discrepancies as shown by the comparative study. This could be further improved by adding additional responses (three, four) with a more diversified nature (acceleration, displacement, etc.);
- Identifiability is influenced by the dependency of calibration parameters on measured responses. This is shown by measurements near singularities, such as supports of the bridge, which present poor identifiability relatively to measurements at the middle of the bridge. This is so because the dependency of the spring on the strain is smaller near supports;
- Temperature variations can be used to perform structural identification and establish uncertainty response baselines;

The methodology can also be expanded to consider multiple parameters, which is a common scenario on civil infrastructures [26, 27, 13].

Only two responses with the same nature have been used, which highlights the relevance of sensor placement. It could be relevant to compare the results of this work with an optimal measurement system design methodology, such as described in [31].

Appendix A. Emulation of numerical models with a Gaussian process

Since a numerical model is typically deterministic in nature and can take hours to compute it is useful to replace it with a probabilistic surrogate model. This current practice is known as metamodeling, or emulation [32]. Examples of this practice in SHM can be found on [27, 26]. Also, applying a metamodel establishes a comprehensive framework for uncertainty analysis which eases the Bayesian inference process.

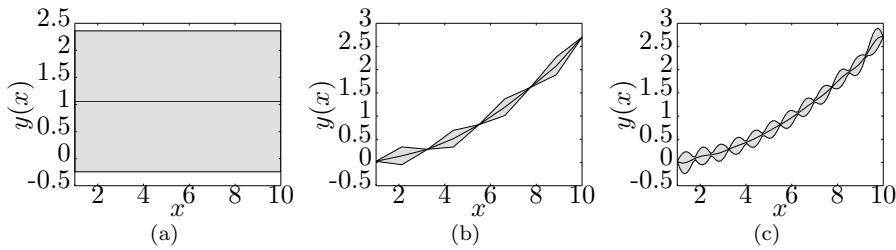


Figure A.10: Prediction interval (grey cloud) and mean function (black line). As more data is being given (from 10(a) to 10(c)) the Gp model interpolates perfectly the input dataset.

In the present work a multiple response Gaussian process (mrGp) [33, 34] shall be used, under the assumption that the response surface of the model $y(x)$ is a single realisation of a spatial random process with a certain prior mean and covariance function. The main requirements for this mrGp are: at a design input

point the mean function should be present and there should be no uncertainty; otherwise the mrGp should reflect a plausible interpolation or extrapolation of the available data, see Fig. A.10.

It is conventioned that in order to approximate the response surface, a dataset of $[\mathbf{X}, \mathbf{Y}]$ with dimensions $[N \times d, N \times q]$ shall be given as input. Dimensions d and q represent the number of input design variables $[\mathbf{x}_1 \ \mathbf{x}_2 \dots \mathbf{x}_d]$ and responses $[\mathbf{y}_1 \ \mathbf{y}_2 \dots \mathbf{y}_q]$, while N is the number of combinations of the whole input space \mathbf{X} and associated \mathbf{Y} . The prior mean function of the mrGp is assumed to belong to a hierarchical structure of linear functions, that in a generalised form can be written as $\mathbf{M}(\mathbf{X}) = \mathbf{H}(\mathbf{X})\boldsymbol{\beta}$, with matrix $\mathbf{H}(\mathbf{X})$ containing N polynomial linear functions $f_{j-1}(x) : j = 1, \dots, p+1$ of degree p (selected by the user) and matrix of regression coefficients $\boldsymbol{\beta}$, for each of the terms contained in matrix $\mathbf{H}(\mathbf{X})$ and each of the q fitted responses \mathbf{Y} .

A typical choice for the prior covariance function which shall also be employed here is the Gaussian form [34]

$$r(x, x') = \sigma_m^2 \exp \left\{ - \sum_{i=1}^d \omega_i (x_i - x'_i)^2 \right\} \quad (\text{A.1})$$

where σ_m^2 is the variance of the response and $\omega_i \ i = 1, \dots, d$ are called roughness parameters or length scales ranges [35] and they represent how roughly the response changes from each training data point to the next.

As proposed by Conti et al.[36] this structure can be generalised to an entire dataset by combining a spatial correlation function and a covariance between responses with the Kronecker product as

$$\mathbf{R}(\mathbf{X}, \mathbf{X}') = \boldsymbol{\Sigma} \otimes \boldsymbol{\Gamma}(\mathbf{X}, \mathbf{X}') \quad (\text{A.2})$$

with $q \times q$ covariance matrix $\boldsymbol{\Sigma}$ and a $N \times N$ correlation matrix $\boldsymbol{\Gamma}$ that contains the squared exponential function of equation A.1 for all the $(\mathbf{X}, \mathbf{X}')$ inputs.

After having supplied a certain amount of data $[\mathbf{X}, \mathbf{Y}]$ to the mrGp (assumed a non-informative prior for $\boldsymbol{\beta}$ and given $\boldsymbol{\omega}$ and $\boldsymbol{\Sigma}$) the posterior distribution of the response at \mathbf{x}_0 is given by

$$\mathbf{y}(\mathbf{x}_0) | \boldsymbol{\Sigma}, \boldsymbol{\omega}, \mathbf{Y} \sim \mathcal{N}(\mathbf{m}^*(\mathbf{x}_0), \boldsymbol{\Sigma} \otimes \boldsymbol{\gamma}^*(\mathbf{x}_0, \mathbf{x}_0)) \quad (\text{A.3})$$

with

$$\mathbf{m}^*(\mathbf{x}_0) = \mathbf{h}(\mathbf{x}_0)\hat{\boldsymbol{\beta}} + \boldsymbol{\gamma}(\mathbf{x}_0)^T \boldsymbol{\Gamma}^{-1}(\mathbf{Y} - \mathbf{H}\hat{\boldsymbol{\beta}}) \quad (\text{A.4})$$

$$\begin{aligned} \boldsymbol{\gamma}^*(\mathbf{x}_o, \mathbf{x}_o) &= \boldsymbol{\gamma}(\mathbf{x}_o, \mathbf{x}_o) - \boldsymbol{\gamma}(\mathbf{x}_o)^T \boldsymbol{\Gamma}^{-1} \boldsymbol{\gamma}(\mathbf{x}_o) + \\ &\quad [\mathbf{h}(\mathbf{x}_0)^T - \mathbf{H}^T \boldsymbol{\Gamma}^{-1} \boldsymbol{\gamma}(\mathbf{x}_0)]^T [\mathbf{H}^T \boldsymbol{\Gamma}^{-1} \mathbf{H}]^{-1} [\mathbf{h}(\mathbf{x}_0)^T - \mathbf{H}^T \boldsymbol{\Gamma}^{-1} \boldsymbol{\gamma}(\mathbf{x}_0)], \end{aligned} \quad (\text{A.5})$$

$\boldsymbol{\gamma}(\mathbf{x}_0)^T = [\boldsymbol{\gamma}(\mathbf{x}_0, \mathbf{x}_1), \dots, \boldsymbol{\gamma}(\mathbf{x}_0, \mathbf{x}_N)]$ as detailed in [37] and $\boldsymbol{\beta}$ is given by solving $\mathbf{H}^T \mathbf{R}^{-1} \mathbf{H} \hat{\boldsymbol{\beta}} = \mathbf{H}^T \mathbf{R}^{-1} \mathbf{Y}$, which corresponds to the linear regression solution of the best linear unbiased predictor.

These relations enforce that when \mathbf{x}_0 coincides with a training data point \mathbf{x}_i , equation number A.3 results in a mean value of $\mathbf{y}(\mathbf{x}_i)$ and a null covariance (see

Fig. A.10). Hence the parameters that characterise the mrGp behaviour (hyperparameters) and that have to be estimated are ω , β and Σ . This is typically done by using maximum likelihood estimates (MLE), mainly for computational reasons.

Appendix B. Gaussian process hyperparameters

The following data represents estimates of parameters, that fully characterise the Gaussian processes, approximated on the modular Bayesian approach. They are named here as hyperparameters ϕ and comprise: a matrix of regression coefficients β , a variance matrix Σ , a noise variance matrix Λ and the roughness parameters ω . The numerical model mrGp has hyperparameters

$$\begin{aligned}\hat{\omega}_{T,K} &= [2.0 \ 1.4] \\ \hat{\beta}_{SB,SG} &= [-0.105 \ 0.121] \quad \hat{\Sigma} = \begin{bmatrix} 3.0645 & 8.4687 \\ 8.4687 & 25.3702 \end{bmatrix}\end{aligned}$$

and the discrepancy function mrGp has hyperparameters

$$\begin{aligned}\hat{\omega}_T &= 6.87 \\ \hat{\beta}_{SB,SG} &= [-3.766 \ -0.242] \quad \hat{\Sigma} = \begin{bmatrix} 22.90 & 1.07 \\ 1.07 & 2.75 \end{bmatrix} \quad \hat{\Lambda} = \begin{bmatrix} 0.27 & 0.03 \\ 0.03 & 0.59 \end{bmatrix}\end{aligned}$$

Acknowledgements

This work was supported by the Engineering and Physical Sciences Research Council (EPSRC) reference number EP/N509796.

Special thanks for the theoretical formulation review is referred to Sergio Jesus and technical support in the aluminium bridge case-study to Zong Tan, Arnett Taylor, Neil Gillespie and Colin Banks.

References

- [1] Jesus AH, Dimitrovová Z, Silva MA. A statistical analysis of the dynamic response of a railway viaduct. *Engineering Structures* 2014;71. doi:[10.1016/j.engstruct.2014.04.012](https://doi.org/10.1016/j.engstruct.2014.04.012).
- [2] Goulet JA, Smith IF. Structural identification with systematic errors and unknown uncertainty dependencies. *Computers & Structures* 2013;128. doi:[10.1016/j.compstruc.2013.07.009](https://doi.org/10.1016/j.compstruc.2013.07.009).
- [3] Erdogan YS, Gul M, Catbas FN, Bakir PG. Investigation of Uncertainty Changes in Model Outputs for Finite-Element Model Updating Using Structural Health Monitoring Data. *Journal of Structural Engineering* 2014;140(11). doi:[10.1061/\(ASCE\)ST.1943-541X.0001002](https://doi.org/10.1061/(ASCE)ST.1943-541X.0001002).
- [4] Capellari G, Eftekhari Azam S, Mariani S. Damage Detection in Flexible Plates through Reduced-Order Modeling and Hybrid Particle-Kalman Filtering. *Sensors* 2015;16(1). doi:[10.3390/s16010002](https://doi.org/10.3390/s16010002).

- [5] Li PJ, Xu DW, Zhang J. Probability-Based Structural Health Monitoring Through Markov Chain Monte Carlo Sampling. *International Journal of Structural Stability and Dynamics* 2015;doi:[10.1142/S021945541550039X](https://doi.org/10.1142/S021945541550039X).
- [6] Lam HF, Yang J, Au SK. Bayesian model updating of a coupled-slab system using field test data utilizing an enhanced Markov chain Monte Carlo simulation algorithm. *Engineering Structures* 2015;102. doi:[10.1016/j.engstruct.2015.08.005](https://doi.org/10.1016/j.engstruct.2015.08.005).
- [7] Simoen E, Roeck GD, Lombaert G. Dealing with uncertainty in model updating for damage assessment: A review. *Mechanical Systems and Signal Processing* 2015;56–57(0). doi:[10.1016/j.ymssp.2014.11.001](https://doi.org/10.1016/j.ymssp.2014.11.001).
- [8] Beck J, Au SK. Bayesian Updating of Structural Models and Reliability using Markov Chain Monte Carlo Simulation. *Journal of Engineering Mechanics* 2002;128(4). doi:[10.1061/\(ASCE\)0733-9399\(2002\)128:4\(380\)](https://doi.org/10.1061/(ASCE)0733-9399(2002)128:4(380)).
- [9] Beck J, Katafygiotis L. Updating Models and Their Uncertainties. I: Bayesian Statistical Framework. *Journal of Engineering Mechanics* 1998;124(4). doi:[10.1061/\(ASCE\)0733-9399\(1998\)124:4\(455\)](https://doi.org/10.1061/(ASCE)0733-9399(1998)124:4(455)).
- [10] Vanik MW, Beck JL, Au SK. Bayesian Probabilistic Approach to Structural Health Monitoring. *Journal of Engineering Mechanics* 2000;126(7). doi:[10.1061/\(ASCE\)0733-9399\(2000\)126:7\(738\)](https://doi.org/10.1061/(ASCE)0733-9399(2000)126:7(738)).
- [11] Cheung S, Beck J. Bayesian Model Updating Using Hybrid Monte Carlo Simulation with Application to Structural Dynamic Models with Many Uncertain Parameters. *Journal of Engineering Mechanics* 2009;135(4). doi:[10.1061/\(ASCE\)0733-9399\(2009\)135:4\(243\)](https://doi.org/10.1061/(ASCE)0733-9399(2009)135:4(243)).
- [12] Behmanesh I, Moaveni B, Lombaert G, Papadimitriou C. Hierarchical Bayesian model updating for structural identification. *Mechanical Systems and Signal Processing* 2015;64-65. doi:[10.1016/j.ymssp.2015.03.026](https://doi.org/10.1016/j.ymssp.2015.03.026).
- [13] Matos JC, Cruz PJ, Valente IB, Neves LC, Moreira VN. An innovative framework for probabilistic-based structural assessment with an application to existing reinforced concrete structures. *Engineering Structures* 2016;111. doi:[10.1016/j.engstruct.2015.12.040](https://doi.org/10.1016/j.engstruct.2015.12.040).
- [14] McFarland J, Mahadevan S. Multivariate significance testing and model calibration under uncertainty. *Computer Methods in Applied Mechanics and Engineering* 2008;197(29-32). doi:[10.1016/j.cma.2007.05.030](https://doi.org/10.1016/j.cma.2007.05.030).
- [15] Higdon D, Gattiker J, Williams B, Rightley M. Computer Model Calibration Using High-Dimensional Output. *Journal of the American Statistical Association* 2008;103(482). doi:[10.1198/016214507000000888](https://doi.org/10.1198/016214507000000888).
- [16] Simoen E, Papadimitriou C, Lombaert G. On prediction error correlation in Bayesian model updating. *Journal of Sound and Vibration* 2013;332(18). doi:[10.1016/j.jsv.2013.03.019](https://doi.org/10.1016/j.jsv.2013.03.019).

- [17] Kuok SC, Yuen KV. Structural health monitoring of Canton Tower using Bayesian framework. SMART STRUCTURES AND SYSTEMS OCT-NOV 2012;10(4-5).
- [18] Kennedy MC, O'Hagan A. Bayesian calibration of computer models. Journal of the Royal Statistical Society: Series B (Statistical Methodology) 2001;63(3). doi:[10.1111/1467-9868.00294](https://doi.org/10.1111/1467-9868.00294).
- [19] Brynjarsdóttir J, O'Hagan A. Learning about physical parameters: The importance of model discrepancy. Inverse Problems 2014;30(11). doi:[10.1088/0266-5611/30/11/114007](https://doi.org/10.1088/0266-5611/30/11/114007).
- [20] Arendt PD, Apley DW, Chen W. Quantification of Model Uncertainty: Calibration, Model Discrepancy, and Identifiability. Journal of Mechanical Design 2012;134(10). doi:[10.1115/1.4007390](https://doi.org/10.1115/1.4007390).
- [21] Yuen KV. Bayesian Methods for Structural Dynamics and Civil Engineering. In: Bayesian Methods for Structural Dynamics and Civil Engineering. John Wiley & Sons, Ltd. ISBN 978-0-470-82456-6; 2010,.
- [22] Arendt PD, Apley DW, Chen W, Lamb D, Gorsich D. Improving Identifiability in Model Calibration Using Multiple Responses. Journal of Mechanical Design 2012;134(10). doi:[10.1115/1.4007573](https://doi.org/10.1115/1.4007573).
- [23] Laory I, Westgate RJ, Brownjohn JMW, Smith IFC. Temperature Variations as Loads Cases for Structural Identification. In: Proceeding of the of 6th International Conference on Structural Health Monitoring of Intelligent Infrastructure (SHMII), Hong-Kong, 2013. Hong Kong; 2013,.
- [24] Laory I, Trinh TN, Smith IF, Brownjohn JM. Methodologies for predicting natural frequency variation of a suspension bridge. Engineering Structures 2014;80. doi:[10.1016/j.engstruct.2014.09.001](https://doi.org/10.1016/j.engstruct.2014.09.001).
- [25] Yarnold MT, Moon FL. Temperature-based structural health monitoring baseline for long-span bridges. Engineering Structures 2015;86(0). doi:[10.1016/j.engstruct.2014.12.042](https://doi.org/10.1016/j.engstruct.2014.12.042).
- [26] Spiridonakos M, Chatzi E. Metamodeling of dynamic nonlinear structural systems through polynomial chaos NARX models. Computers & Structures 2015;157. doi:[10.1016/j.compstruc.2015.05.002](https://doi.org/10.1016/j.compstruc.2015.05.002).
- [27] Wan HP, Ren WX. Parameter Selection in Finite-Element-Model Updating by Global Sensitivity Analysis Using Gaussian Process Metamodel. JOURNAL OF STRUCTURAL ENGINEERING 2015;141(6). doi:[10.1061/\(ASCE\)ST.1943-541X.0001108](https://doi.org/10.1061/(ASCE)ST.1943-541X.0001108).
- [28] Liu F, Bayarri MJ, Berger JO. Modularization in Bayesian analysis, with emphasis on analysis of computer models. Bayesian Analysis 2009;4(1). doi:[10.1214/09-BA404](https://doi.org/10.1214/09-BA404).

- [29] Kennedy MC, O'Hagan A. Supplementary details on Bayesian Calibration of Computer Models. Tech. Rep.; 2001.
- [30] Swanson Analysis Systems IP I. ANSYS, Inc. Documentation for Release 15.0. 2013.
- [31] Arendt PD, Apley DW, Chen W. A preposterior analysis to predict identifiability in the experimental calibration of computer models. IIE Transactions 2016;48(1). doi:[10.1080/0740817X.2015.1064554](https://doi.org/10.1080/0740817X.2015.1064554).
- [32] Lophaven SN, Nielsen HB, Søndergaard J. DACE - A MATLAB Kriging Toolbox. 2002.
- [33] O'Hagan A. Bayesian analysis of computer code outputs: A tutorial. Reliability Engineering & System Safety 2006;91(10-11). doi:[10.1016/j.ress.2005.11.025](https://doi.org/10.1016/j.ress.2005.11.025).
- [34] Rasmussen CE, Williams CKI. Gaussian Processes for Machine Learning. Adaptive computation and machine learning; Cambridge, Mass: MIT Press; 2006. ISBN 978-0-262-18253-9.
- [35] Cressie NAC. Statistics for Spatial Data. Wiley series in probability and mathematical statistics; reviewed ed.; New York: Wiley; 1993. ISBN 978-0-471-00255-0.
- [36] Conti S, O'Hagan A. Bayesian emulation of complex multi-output and dynamic computer models. Journal of Statistical Planning and Inference 2010;140(3). doi:[10.1016/j.jspi.2009.08.006](https://doi.org/10.1016/j.jspi.2009.08.006).
- [37] Conti S, Gosling JP, Oakley JE, O'Hagan A. Gaussian process emulation of dynamic computer codes. Biometrika 2009;96(3). doi:[10.1093/biomet/asp028](https://doi.org/10.1093/biomet/asp028).